

# An algorithm for calculating the Lorentz angle in silicon detectors

V. Bartsch<sup>a</sup> W. de Boer<sup>a</sup> J. Bol<sup>a</sup> A. Dierlamm<sup>a</sup> E. Grigoriev<sup>a</sup>  
F. Hauler<sup>a</sup> S. Heising<sup>a,b</sup> L. Jungermann<sup>a</sup>

<sup>a</sup>*Institut für Experimentelle Kernphysik, Universität Karlsruhe (TH), P.O. Box  
6980, 76128 Karlsruhe, Germany*

<sup>b</sup>*European Laboratory for Particle Physics (CERN), CH-1211 Geneva 23,  
Switzerland*

---

## Abstract

Future experiments will use silicon sensors in the harsh radiation environment of the LHC (Large Hadron Collider) and high magnetic fields. The drift direction of the charge carriers is affected by the Lorentz force due to the high magnetic field. Also the resulting radiation damage changes the properties of the drift.

In this paper measurements of the Lorentz angle of electrons and holes before and after irradiation are reviewed and compared with a simple algorithm to compute the Lorentz angle.

*Key words:* silicon, sensors, detectors, Lorentz angle, magnetic field, CMS

---

## 1 Introduction

The Lorentz angle  $\Theta_L$ , by which charge carriers are deflected in a magnetic field perpendicular to the electric field, is defined by:

$$\tan(\Theta_L) = \frac{\Delta x}{d} = \mu_H B = r_H \mu B, \quad (1)$$

where  $d$  corresponds to the drift distance along the electric field and  $\Delta x$  to the shift of the signal position (see Fig. 1). If the ionization is produced at the surface, the drift distance equals the detector thickness. If the ionization is produced homogeneously by a traversing particle, the averaged drift distance is only half the detector thickness. The Hall mobility is denoted by  $\mu_H$ , the drift mobility by  $\mu$ . The Hall mobility in a magnetic field differs from the drift

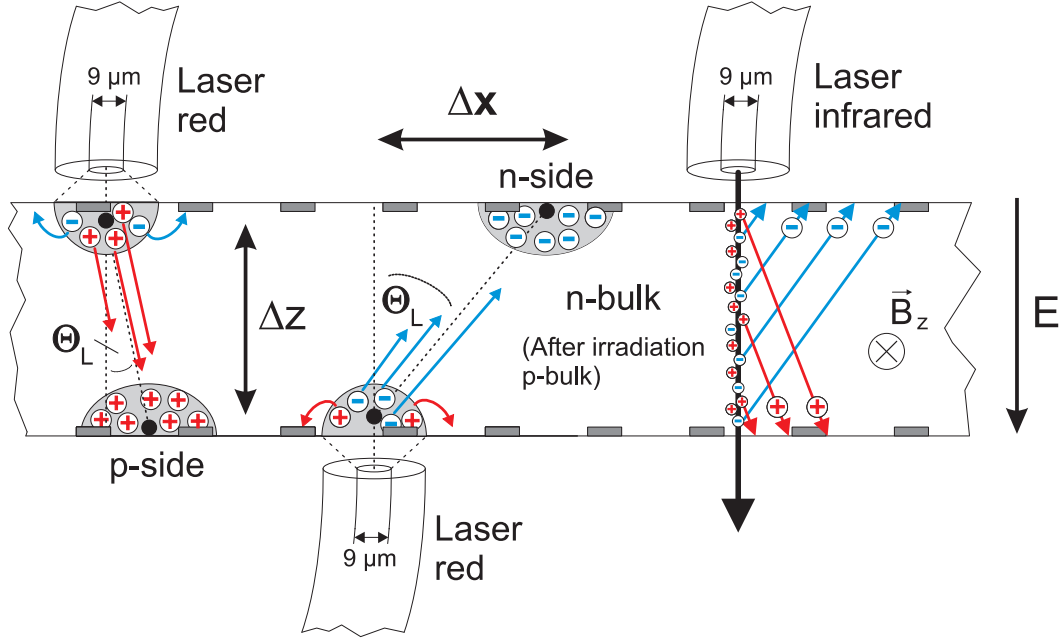


Fig. 1. The figure shows the principle of the Karlsruhe setup to measure the Lorentz angle of holes and electrons (6). It is equipped with three fibers delivering laser light to the silicon. The red lasers have a penetration depth of a few  $\mu\text{m}$ , so with a laser pulse on the n-side or p-side one can measure the drift of electrons and holes, respectively. The infrared laser generates charge throughout the whole thickness of the detector.

mobility without magnetic field by the Hall scattering factor  $r_H$ . This factor describes the mean free time between carrier collisions, which depends on the carrier energy (1). The Hall scattering factor has a value of  $\approx 0.7$  for holes and  $\approx 1.15$  for electrons at room temperature (2). The mobility  $\mu$  increases with temperature proportional to  $T^{-2.5}$  for holes and  $T^{-2.2}$  for electrons as shown by measurements (3). For the high purity sensors used for particle detection (dopings  $< 10^{13}\text{cm}^{-3}$ ) the mobility is independent of the doping concentration (4; 5). The hole mobility is about  $470\text{cm}^2/\text{Vs}$  at 300 K, the electron mobility is about  $1417\text{cm}^2/\text{Vs}$  at 300 K. Thus the drift mobility of electrons is about three times larger than the hole mobility. Therefore the Lorentz shift is considerably larger for electrons than for holes and consequently the p-side read out shows a smaller Lorentz shift than the n-side read out. Still the Lorentz shifts for holes generated at the surface reach about  $40\ \mu\text{m}$  ( $70\ \mu\text{m}$ ) in a 4 T magnetic field for a  $320\ \mu\text{m}$  ( $500\ \mu\text{m}$ ) thick detector, so that the shifts should be accounted for. From the right hand side of Fig. 1 it is clear that a minimum ionising particle (MIP) yields a broader signal for electrons (n-side) than for holes (p-side). Another important question is the dependence of the Lorentz shift on the irradiation dose. The change of drift mobility and electric field in the silicon detector due to defects introduced by radiation damage results in a change of the Lorentz shift and thus of the alignment of the detector.

## 2 Experimental results

A comprehensive study of Lorentz shifts of non-irradiated and irradiated sensors was performed at Karlsruhe (6; 7; 8; 9). The Lorentz angle has been measured for electrons and holes separately. A temperature range of 77 K-300 K was covered. The Lorentz angle is measured by injecting charges at the surface on one side and observing the drift through the sensor by measuring the position of the charge on the opposite side (see Fig. 1). Alternative methods are described in (10; 11).

Charges are generated by injecting laser light with a wavelength of  $\lambda \approx 650$  nm, which has an absorption length of  $\approx 3 \mu\text{m}$  at 300 K. In this case charge carriers of one type are collected at the nearest electrode, whereas the carriers of the other type drift towards the opposite side. This allows the measurement of the Lorentz angle for electrons and holes separately by injecting laser light either on the p- or n-side. To simulate a MIP an infrared laser with a wavelength of 1060 nm was used, which has an absorption length of  $\approx 300 \mu\text{m}$  at room temperature. Both lasers from Fermions Lasertech (12) have a maximum power of 1 mW, which could be regulated with the pulse height and width of the input pulse to the laserdiodes. Typically a laser pulse with a width around 1 ns was generated. The laser pulse was sent to the sensor via a single-mode fibre with an inner diameter of a few microns. So the beam spot on the detector could be varied from a few micron onwards by changing the difference between fibre and sensor.

For the measurements the JUMBO magnet from the Forschungszentrum Karlsruhe (13) was used in a  $B \leq 10$  T configuration with a warm bore of 72 mm. The sensors are double sided “baby” detectors of approximately 2x1 cm from the HERA-B production by Sintef (14). They have a strip pitch of  $50 \mu\text{m}$  on the p-side and  $80 \mu\text{m}$  on the n-side; the strips on opposite sides are oriented at an angle of  $90^\circ$  with respect to each other. The capacitively coupled read out strips are connected through a  $1 \text{ M}\Omega$  resistor to the bias ring. The read out chip for the strip detectors is the Premux128-Chip with a shaping time of 45 ns (15). The chip’s common mode is suppressed by a double correlated sampling technique, which subtracts the signal’s baseline. The threshold could be adjusted but the signal to noise ratio from the laser pulse, corresponding to a few times the signal from a minimum ionizing particle (MIP), was sufficiently high, so that the thresholds were not critical.

The averaged signal position  $\bar{x}$  is computed from either a fit with the sum of two Gaussians or from the center of gravity of the pulses  $p_i$  on neighbouring strips  $x_i$ , i.e.  $\bar{x} = \sum p_i \cdot x_i / \sum p_i$ . Both methods gave comparable results.

Our measurements showed that the Lorentz shift with the magnetic field are

Table 1

The Lorentz shift  $\Delta x$  for holes generated at the surface for a 300  $\mu\text{m}$  thick sensor in a 4 T magnetic field as function of bias voltage for a non-irradiated sensor and an irradiated sensor. The sensor was irradiated with 21 MeV protons up to a fluence of  $10^{13}$  p/cm<sup>2</sup>. The full depletion voltages are 40 V (100 V) for the non-irradiated sensor (irradiated) sensor.  $\Theta_{\text{sim}}$  was obtained from the algorithm discussed in Section 3.

| non-irradiated            |   |   |  |   | irradiated with $10^{13}$ 21 MeV p/cm <sup>2</sup> |   |  |   |
|---------------------------|---|---|--|---|--|---|--|---|
| $U_{\text{bias}}$<br>in V | $\Delta x$<br>in $\mu\text{m}$<br>(270 K) | $\Delta x$<br>in $\mu\text{m}$<br>(260 K) | $\Theta_{\text{meas}}$<br>in $^\circ$<br>(270 K) | $\Theta_{\text{sim}}$<br>in $^\circ$<br>(270 K) | $U_{\text{bias}}$<br>in V                          | $\Delta x$<br>in $\mu\text{m}$<br>(260 K) | $\Theta_{\text{meas}}$<br>in $^\circ$<br>(260 K) | $\Theta_{\text{sim}}$<br>in $^\circ$<br>(260 K) |
| 100                       | $38 \pm 2$                                | $41 \pm 2$                                | $7.2 \pm 0.4$                                    | 7.2   | 100  | $42 \pm 3$                                | $8.0 \pm 0.5$                                    | 7.8   |
| 200                       | $31 \pm 2$                                | $34 \pm 2$                                | $5.9 \pm 0.3$                                    | 6.1   | 150  | $40 \pm 2$                                | $7.6 \pm 0.5$                                    | 7.2   |
| 300                       | $25 \pm 1$                                | $28 \pm 2$                                | $4.8 \pm 0.2$                                    | 5.3   |  |   |  |   |

linear up to 9 T (6), which means that Eq. 1 can be used. Before irradiation the sensor depletes fully at a bias voltage of 40 V, while after irradiation with  $1.0 \cdot 10^{13}$  21 MeV protons/cm<sup>2</sup> the depletion voltage has increased to 100 V. This implies that the bulk is inverted from n-type to p-type material, as expected (16). The bulk damage of 21 MeV protons is about 2.1 times the damage from 1 MeV neutrons (17). Numerical results on the Lorentz angles and shifts have been summarized in Tables 1 and 2 and are displayed in Figs. 2 and 3 before and after irradiation, respectively.

The Lorentz shift for holes is not strongly depending on irradiation as shown in Fig. 2, while for electrons there is a clear dependence on the irradiation dose as shown in Fig. 3 and Table 2. The calculated values in the Tables and

Table 2

As Table 1, but now for electrons instead of holes.

| non-irradiated            |   |  |   | irradiated with $10^{13}$ 21 MeV p/cm <sup>2</sup> |   |  |   |
|---------------------------|---|--|---|--|---|--|---|
| $U_{\text{bias}}$<br>in V | $\Delta x$<br>in $\mu\text{m}$<br>(280 K) | $\Theta_{\text{meas}}$<br>in $^\circ$<br>(280 K) | $\Theta_{\text{sim}}$<br>in $^\circ$<br>(280 K) | $U_{\text{bias}}$<br>in V                          | $\Delta x$<br>in $\mu\text{m}$<br>(280 K) | $\Theta_{\text{meas}}$<br>in $^\circ$<br>(280 K) | $\Theta_{\text{sim}}$<br>in $^\circ$<br>(280 K) |
| 40                        | $192 \pm 11$                              | $33 \pm 2$                                       | 32  | 50   | $117 \pm 7$                               | $21 \pm 1$                                       | 20  |
| 100                       | $170 \pm 10$                              | $30 \pm 2$                                       | 27  | 100  | $127 \pm 7$                               | $23 \pm 1$                                       | 25  |
|                           |   |  |   | 150  | $126 \pm 7$                               | $23 \pm 1$                                       | 22  |

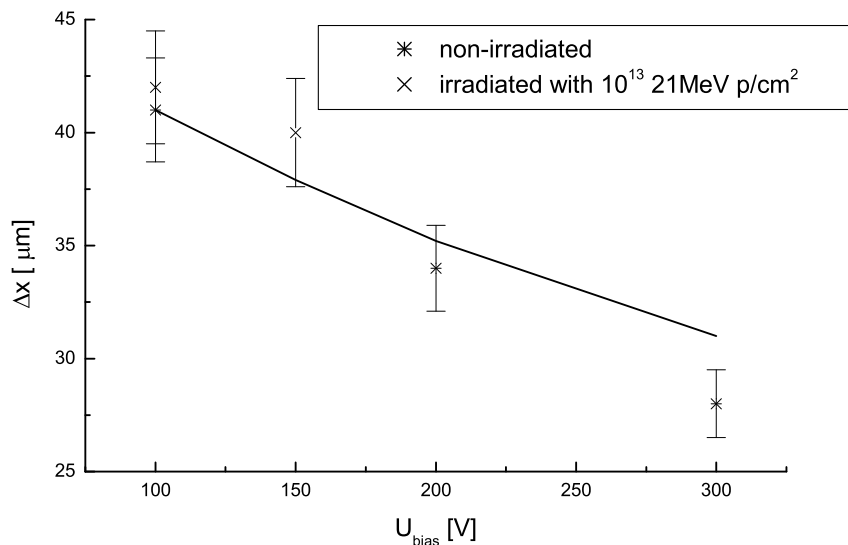


Fig. 2. The Lorentz shift  $\Delta x$  for holes generated at the surface for a  $300\ \mu\text{m}$  thick sensor in a  $4\ \text{T}$  magnetic field versus bias voltage  $U_{\text{bias}}$ . The bars represent systematic errors. The temperature is  $260\ \text{K}$ . The line is calculated from the algorithm discussed in the text.

Figures are discussed in the next section. The strong decrease of the Lorentz shift for electrons after irradiation for bias voltages below  $100\ \text{V}$  originates from the fact that the detector is not depleted anymore for these voltages, thus reducing the effective thickness, as will be discussed in section 4.

### 3 Algorithm for the Lorentz angle at full depletion

In single sided silicon strip detectors with read-out on the p-side the holes are the ones collected. It is expected that the maximum bias voltage after 10 years of LHC will be below the breakdown voltage of at least  $500\ \text{V}$ . So the strip detectors can run at full depletion. For pixel detectors this is not the case as will be discussed in Sect. 4.

#### 3.1 Non-irradiated sensors

Algorithms for the Lorentz shift will first be discussed for non-irradiated sensors and then conclusions for irradiated detectors will be drawn. The mobility  $\mu(E)$  is proportional to the mobility at low electric field  $\mu_{\text{low}}$  and its behaviour at high electric fields is described with the help of a saturation velocity  $v_{\text{sat}}$

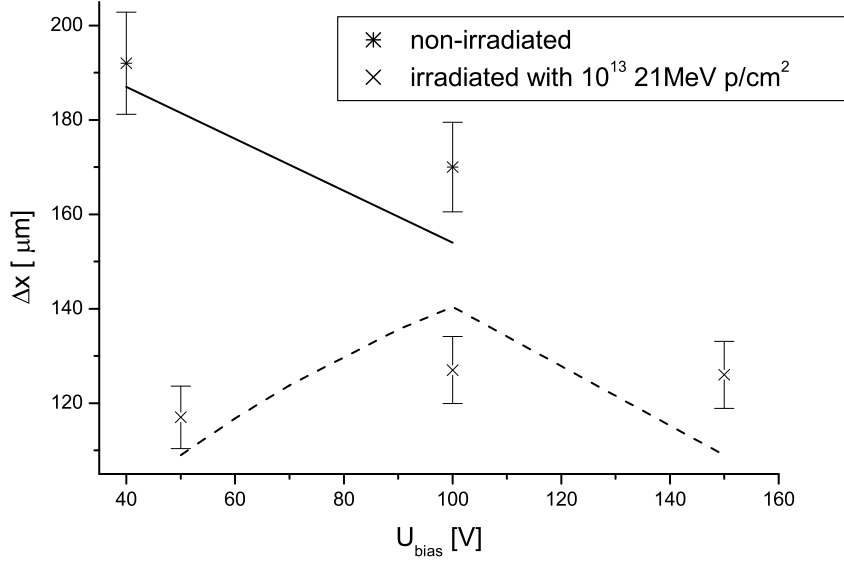


Fig. 3. The Lorentz shift  $\Delta x$  for electrons generated at the surface for a  $300 \mu\text{m}$  thick sensor in a  $4 \text{ T}$  magnetic field versus bias voltage  $U_{\text{bias}}$ . The bars represent systematic errors. The temperature is  $280 \text{ K}$ . The lines are calculated from the algorithm discussed in the text.

(3):

$$\mu(E) = \frac{\mu_{\text{low}}}{\left(1 + \left(\frac{\mu_{\text{low}} E}{v_{\text{sat}}}\right)^\beta\right)^{\frac{1}{\beta}}} \quad (2)$$

For holes the parameter values used are:  $\mu_{\text{low}} = 470.5 \frac{\text{cm}^2}{\text{Vs}} \cdot (T/300)^{-2.5}$ ;  $\beta = 1.213 \cdot (T/300)^{0.17}$ ;  $v_{\text{sat}} = 8.37 \cdot 10^6 \text{ cm/s} \cdot (T/300)^{0.52}$ , while for electrons the following values are used:  $\mu_{\text{low}} = 1417 \frac{\text{cm}^2}{\text{Vs}} \cdot (T/300)^{-2.2}$ ;  $\beta = 1.109 \cdot (T/300)^{0.66}$ ;  $v_{\text{sat}} = 1.07 \cdot 10^7 \text{ cm/s} \cdot \left(\frac{T}{300}\right)^{0.87}$ .

To calculate the Lorentz shift one has to divide the sensor into several zones and then compute the shifts in each zone at an average electric field. The total shift is the sum of the shifts in each zone. The electric field depends on the  $z$ -position, the bias voltage, the full depletion voltage  $U_{\text{depl}}$  and the thickness of the sensor:

$$E(z) = \frac{U_{\text{bias}} - U_{\text{depl}}}{d} + \frac{2 \cdot U_{\text{depl}}}{d} \cdot \left(1 - \frac{z}{d}\right) \quad (3)$$

As can be seen from Fig. 4 the trajectory of electrons is more strongly curved than the one for holes. For holes one needs only one zone with a mean electric

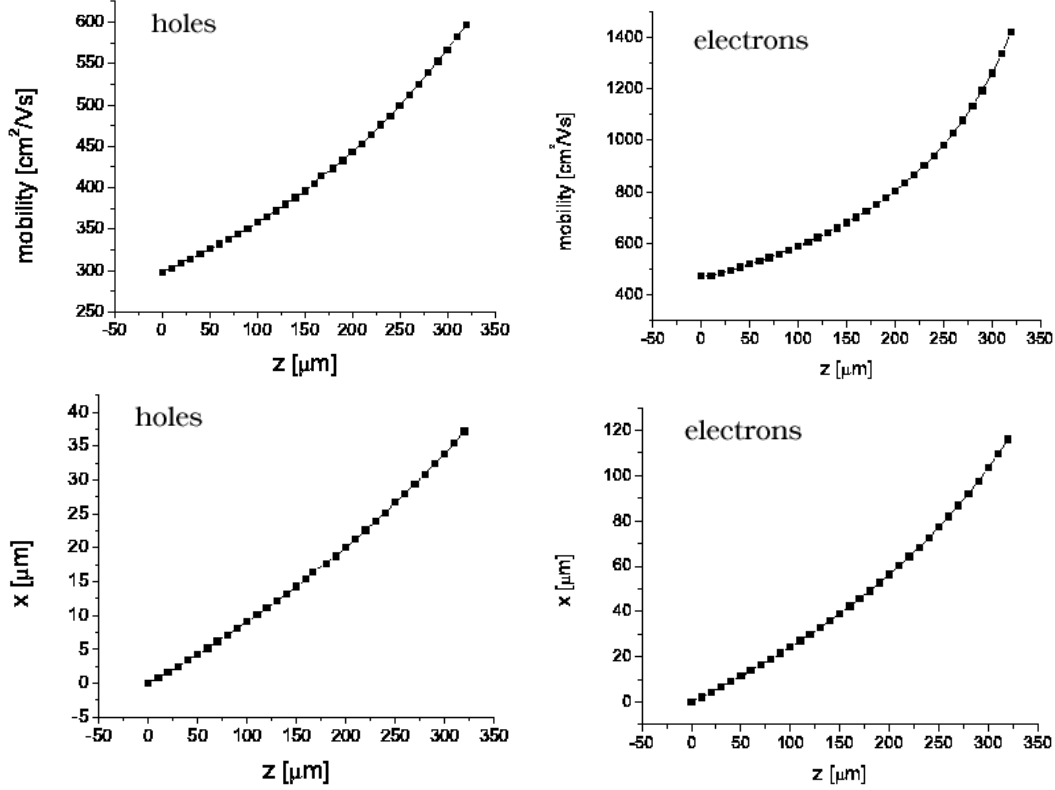


Fig. 4. Simulated mobility (top curve) and mean trajectory (lower figure) of holes (left hand side) and electrons (right hand side) at a full depletion voltage of 280 V and a bias voltage of 350V at a temperature of 263 K in a 4 T magnetic field. The thickness is 320 μm. The total Lorentz shift for holes is 37 μm, for electrons 116 μm, the total shift calculated with a mean electric field for holes is 36 μm, for electrons 104 μm.

field  $E_{\text{mean}}$ , which depends only on the applied bias voltage  $U_{\text{bias}}$ :

$$E_{\text{mean}} = \frac{E(x=0) + E(x=d)}{2} = \frac{U_{\text{bias}}}{d} \quad (4)$$

Given the electric field, one can calculate the mobility from Eq. 2 and the corresponding Lorentz shift from Eq. 1. Table 1 shows that the calculations match the measurements quite well.

The temperature dependence of the Lorentz shift is shown in Fig. 5. The Lorentz shift varies about 5 μm for a 300 μm thick sensor at 100 V in a 4 T magnetic field, if the temperature is varied between 250 K and 270 K, for both electrons and holes.

Fig. 6 shows the calculated Lorentz angle as a function of the bias voltage. The dependence is quite linear for fully depleted sensors. Instead of calculating the Lorentz angle from the mobility one can use the approximate linearity between

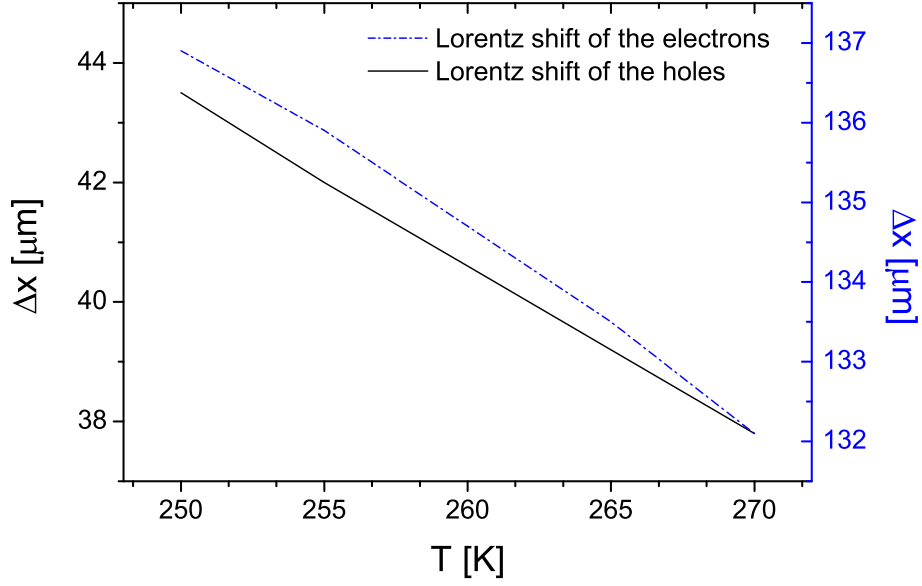


Fig. 5. The temperature dependence of the Lorentz shift  $\Delta x$  for holes (lower curve, left scale) and electrons (top curve, right scale) predicted for a  $300\ \mu\text{m}$  thick sensor in a  $4\text{ T}$  magnetic field at a bias voltage  $U_{\text{bias}}$  of  $100\text{ V}$ .

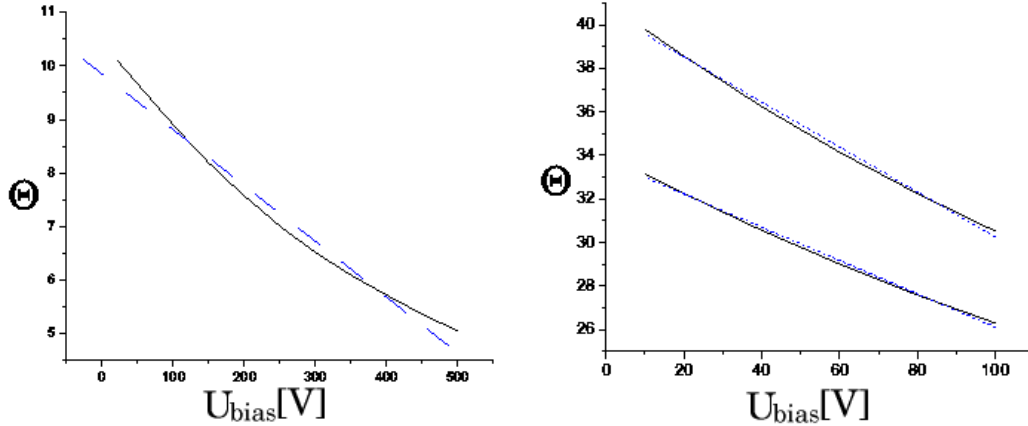


Fig. 6. The Lorentz angle  $\theta$  for holes (left hand side) and electrons (right hand side) simulated for a  $320\ \mu\text{m}$  thick sensor in a  $4\text{ T}$  magnetic field by Eqs. 1, 2 and 4. The dashed lines represent the linear approximation. The Lorentz angle for electrons (right hand side) has been calculated for a mobility  $\mu_{\text{low}}$  of  $1417\text{ cm}^2/\text{Vs}$  (top curve) and  $1100\text{ cm}^2/\text{Vs}$  (lower curve), where the latter mobility is typical for irradiated sensors.

bias voltage and Lorentz angle, which can be written as

- $\Theta = 9.85^\circ - 0.01 \cdot U_{\text{bias}}$  for holes,
- $\Theta = 40.59^\circ - 0.10 \cdot U_{\text{bias}}$  for electrons with a mobility  $\mu_{\text{low}}$  of  $1417\text{ cm}^2/\text{Vs}$  and a bias voltage below  $100\text{ V}$ ,

- $\Theta = 33.75^\circ - 0.08 \cdot U_{\text{bias}}$  for electrons with a mobility  $\mu_{\text{low}}$  of  $1100 \text{ cm}^2/\text{Vs}$  and a bias voltage below  $100\text{V}$ .

### 3.2 Irradiated sensors

There are three main parameters, which change after irradiation: the mobility, the electric field and the depletion voltage. As long as the sensor is fully depleted and - this becomes relevant for electrons - the bias voltage is low, Eqs. 1, 2 and 4 can be used to calculate the Lorentz shift. The precise knowledge of the depletion voltage is not needed in this case. For higher bias voltages the saturation of the drift velocity has to be taken into account, at least for electrons, which implies the use of several zones inside the sensor and Eq. 3 instead of 4 has to be used, which depends on the depletion voltage. Also the Hall scattering factor might change after irradiation, but in this paper the Hall scattering factor is assumed to be independent of radiation damage. So only the dependence of the mobility and the electric field on the radiation dose have to be discussed.

The dependence of the mobility on the irradiation dose is still controversial. In Ref.(22) no significant changes were observed in the transport properties of both electrons and holes up to  $0.5 \cdot 10^{14} \text{ 1 MeV n/cm}^2$  and a prediction is made that a fluence of at least about  $10^{15} \text{ 1 MeV n/cm}^2$  is necessary to affect carrier drift mobilities significantly. In Ref. (23) the mobility for both carrier types in irradiated sensors agree with those for the non-irradiated sensor within the errors for fluences up to  $2 \cdot 10^{14} \text{ 1 MeV n/cm}^2$ . In contrast a change of mobility after irradiation for holes and electrons was observed in Ref. (24):

- The mobility  $\mu_{\text{low}}$  of holes changes slightly from  $470 \text{ cm}^2/\text{Vs}$  to about  $460 \text{ cm}^2/\text{Vs}$  after irradiation to a fluence of  $10^{13} \text{ 1 MeV n/cm}^2$ . Above this fluence the mobility does not change any more. The change of mobility corresponds to a change in the Lorentz shift of a few percent.
- The mobility  $\mu_{\text{low}}$  of the electrons changes more significantly from  $1417 \text{ cm}^2/\text{Vs}$  to  $1000 \text{ cm}^2/\text{Vs}$ . The reduction of the mobility is so strong that one has to take this into account when computing the Lorentz shift.

This agrees with the measurements of Lorentz shift for electrons done in Karlsruhe. As demonstrated in Table 3 the data of the irradiated sensor can be well explained with the help of a reduced mobility  $\mu_{\text{low}}$ .

In an irradiated sensors the so-called double junction effect arises (see for example Ref. (25) and (26)). This effect has been observed and modelled for a specific sensor using data from TCT (Transient Current Technique) measurements (27). A trend can be observed that with higher bias voltages the double

Table 3

The Lorentz shift  $\Delta x$  for electrons generated at the surface for a  $300\mu\text{m}$  thick sensor in a  $4\text{ T}$  magnetic field at  $280\text{ K}$  as function of bias voltage. The sensor was irradiated with  $21\text{ MeV}$  protons up to a fluence of  $10^{13}\text{ cm}^2$ . The full depletion voltage is  $100\text{ V}$ .  $\Theta_{\text{sim}}$  with the reduced mobility fits the data  $\Theta_{\text{meas}}$  better.

| $U_{\text{bias}}$<br>in V | $\Delta x$<br>in $\mu\text{m}$ | $\Theta_{\text{meas}}$<br>in $^\circ$ | $\Theta_{\text{sim}}$ in $^\circ$<br>$\mu_{\text{low}} = 1417\text{ cm}^2/\text{Vs}$<br>at $300\text{ K}$ | $\Theta_{\text{sim}}$ in $^\circ$<br>$\mu_{\text{low}} = 1100\text{ cm}^2/\text{Vs}$<br>at $300\text{ K}$ |
|---------------------------|--------------------------------|---------------------------------------|---|---|
| 50                        | $117 \pm 7$                    | $21 \pm 1$                            | 24  | 20  |
| 100                       | $127 \pm 7$                    | $23 \pm 1$                            | 29  | 25  |
| 150                       | $126 \pm 7$                    | $23 \pm 1$                            | 25  | 22  |

junction effect is less pronounced. At bias voltages, which are equal or higher than the depletion voltage, the double junction effect is negligible. Since strip sensors to be used for the LHC can be biased well above the depletion voltage, the double junction effect should be small.

#### 4 Algorithm for the Lorentz angle at high irradiation doses

Pixel detectors are located near the beam pipe and therefore have to stand higher radiation doses than strip detectors. It is not guaranteed that they can be always fully depleted. Since the bulk inverts after strong irradiation from n-type to p-type, the pn-junction will be on the n-side and the depletion starts from the n-side. If not fully depleted, the charge will not reach the p-side. Therefore the readout is preferentially on the n-side(21), thus collecting electrons. This influences the Lorentz shift, because the drift length of the electrons is shortened and therefore the Lorentz shift will be reduced, as indicated in Fig. 7. Our algorithm is compared with measurements for the ATLAS pixel sensor reported in Ref. (11). The ATLAS pixel sensors are  $280\mu\text{m}$  thick and have a full depletion voltage before irradiation of about  $150\text{ V}$ . The magnetic field during the measurements was  $1.4\text{ T}$  and the temperature  $300\text{ K}$  for the non-irradiated sensors and  $263\text{ K}$  for the irradiated sensors. The measured values are compared to the simulated values in Table 4.

The electric field in the pixel sensor changes more than in the strip sensor, if they are not fully depleted after irradiation. In that case the mobility of the electrons varies appreciably as can be seen in Fig. 8. Therefore the algorithm divides the  $z$ -axis of the sensor into five parts. In each part the averaged mobility and corresponding Lorentz shift was calculated using the standard and reduced mobilities  $\mu_{\text{low}}$  of Table 3 and the total Lorentz shift is the sum of the shifts in the five parts, while the Lorentz angle is an effective Lorentz

Table 4

The Lorentz angle for electrons for a  $280\ \mu\text{m}$  thick sensor in a  $1.4\ \text{T}$  magnetic field. The full depletion voltage before irradiation is  $150\ \text{V}$ . The measured data are taken from (11). The algorithm used for the simulation divides the sensor into five parts, in which the mean electric field and the corresponding Lorentz shift are calculated. The averaged Lorentz angle is defined to be the arc tangent of the total Lorentz shift divided by the depletion depth.  $\Theta_{\text{sim}}$  with the reduced mobility fits the data  $\Theta_{\text{meas}}$  better.

| Fluence<br>$\text{n}/\text{cm}^2$ | $U_{\text{bias}}$<br>in V | Depl. depth<br>in $\mu\text{m}$ | $\Theta_{\text{meas}}$<br>in $^\circ$ | $\Theta_{\text{sim}}$ in $^\circ$<br>$\mu_{\text{low}} = 1417\ \text{cm}^2/\text{Vs}$<br>at 300 K | $\Theta_{\text{sim}}$ in $^\circ$<br>$\mu_{\text{low}} = 1100\ \text{cm}^2/\text{Vs}$<br>at 300 K |
|-----------------------------------|---------------------------|---------------------------------|---------------------------------------|---|---|
| 0                                 | 150                       | $283 \pm 6$                     | $9.0 \pm 0.9$                         | 8.4   |   |
| $5 \cdot 10^{14}$                 | 150                       | $123 \pm 19$                    | $5.9 \pm 1.3$                         | 6.7   | 5.7   |
| $5 \cdot 10^{14}$                 | 600                       | $261 \pm 8$                     | $2.6 \pm 0.5$                         | 4.4   | 3.9   |
| $10^{15}$                         | 600                       | $189 \pm 12$                    | $3.1 \pm 1.0$                         | 3.8   | 3.5   |
| $10^{15}$                         | 600                       | $217 \pm 13$                    | $2.7 \pm 0.8$                         | 3.2   | 3.0   |

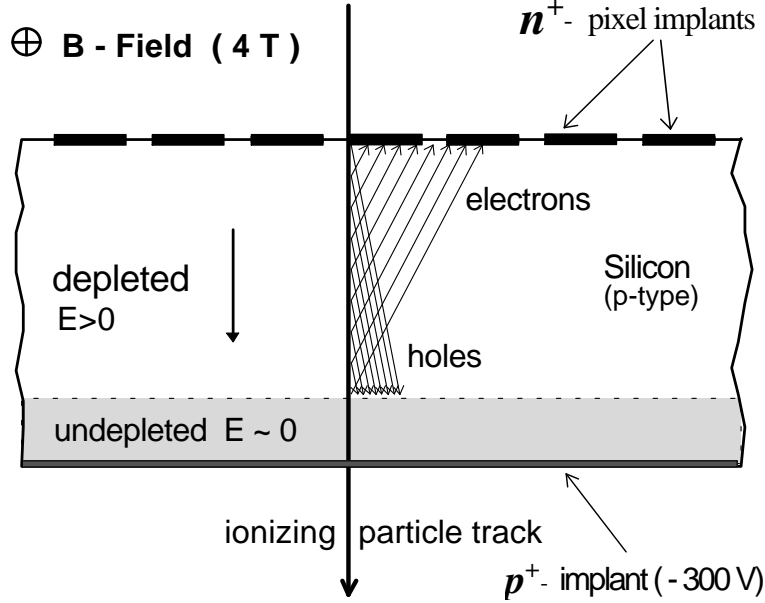


Fig. 7. After type inversion the sensor depletes from the  $n$ -pixel side. With increasing radiation dose the sensor cannot be fully depleted and the total Lorentz shift is reduced. (18)

angle, defined by the shift and the drift distance in the detector. Comparing the simulations with the measurements one observes that the data can be fitted better with lower mobilities after irradiation, as expected from the discussion in Sect.3.2. So it has been shown that the proposed algorithm also works for the pixel detectors, if the reduced drift length is taken into account.

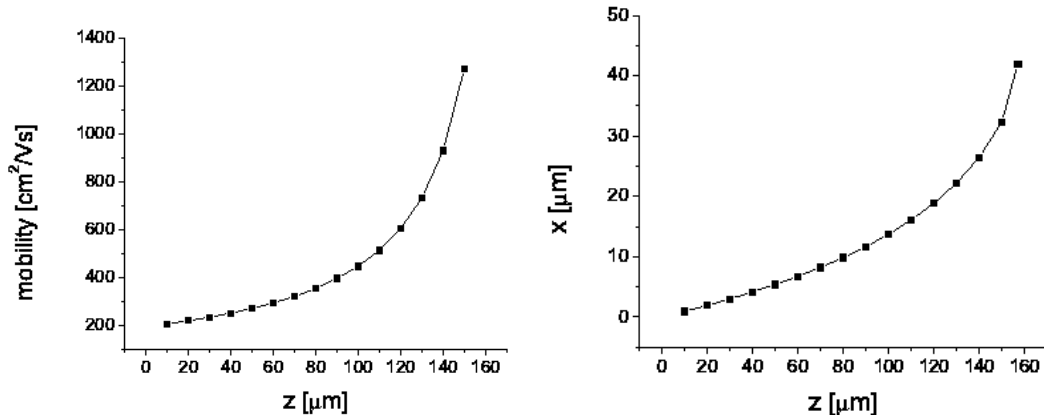


Fig. 8. Simulated mobility (left hand side) and mean trajectory (right hand side) of electrons at a full depletion voltage of 1100 V and a bias voltage of 300 V at 263 K change strongly in the depleted zone of the sensor.

## 5 Summary

The Lorentz angle is determined by electric and magnetic fields and can be modelled by Eqs. 1, 2 and 3 or 4. Because of the different mobility and Hall scattering factor for holes and electrons, the Lorentz shift for electrons is at least four times the one for holes. Irradiation decreases the electron mobility at low electric fields  $\mu_{\text{low}}$  significantly. The hole mobility is hardly affected by irradiation.

The simulated data have been compared with measured values from HERA-B test structures and the ATLAS pixel sensor. It has been shown that the algorithms developed here simulate the Lorentz shifts reasonably well, if one takes into account the reduced electron mobility after irradiation.

## Acknowledgements

This work was done within the framework of the RD39 Collaboration (28). We thank Iris Abt for supplying us with double sided mini-strip detectors.

## References

- [1] R.A. Smith, Semiconductors, *Cambridge Univ. Press*, 1968.
- [2] Landolt-Börnstein, *Numerical Data and Functional Relationships in Science and Technology*, Group III, Vol. **17a**, Springer Verlag, Berlin, 1982.
- [3] C.Canali et al., Electron and hole drift velocity measurements in silicon

- and their empirical relation to electric field and temperature, *IEEE Trans. on Electron Devices*, Vol.**ED-22**, 1045–47, 1975.
- [4] G. Masetti et al., Modelling of carrier mobility against carrier concentration in Arsenic-, Phosphorus- and Boron-doped silicon, *IEEE Trans. on Electron Devices*, Vol.**ED-30**, 764–69, 1983.
- [5] N.D. Arora et al., Electron and hole mobilities in silicon as a function of concentration and temperature, *IEEE Trans. on Electron Devices*, Vol.**ED-29**, 292–295, 1982.
- [6] W. de Boer et al., Lorentz angle measurements in irradiated silicon detectors between 77K and 300K, *NIM A* **461** (2001), 200,  
V. Bartsch et al., *NIM A* **478** (2002), 330.
- [7] F. Röderer, Messung von Lorentz-Winkeln in Silizium-Detektoren, Diplomarbeit, Univ. of Karlsruhe, IEKP-KA/98–24 (in german only).
- [8] S. Heising, Silicon detectors for high energy physics experiments at low temperatures and high magnetic fields, Ph. D. thesis. Univ. of Karlsruhe, IEKP-KA/99–26 (in german only).
- [9] F. Hauler, Lorentzwinkelmessungen an bestrahlten Silizium-Streifendetektoren im Temperaturbereich T=77-300K, Diplomarbeit, Univ. of Karlsruhe, IEKP-KA/2000–12 (in german only).
- [10] E. Belau et al., Charge Collection in Silicon Strip Detectors, *NIM A* **214** (1983) 253.
- [11] M. Aleppo, A measurement of Lorentz angle of radiation-hard pixel sensors, *NIM A* **465**(2001), 108–111.
- [12] <http://www.fermions.com>
- [13] F. Hornung, A. Rimikes, Th. Schneider, High Magnetic Field facilities and Projects at the Forschungszentrum Karlsruhe, Internal Note, 1999.
- [14] I. Abt et al., Cluster shapes and cluster sizes in the HERA-B silicon vertex detector, *NIM A* **469**(2001), 147–158
- [15] L.L. Jones, PreMux128 Specification version 2.3, Rutherford Internal Note, 1995.
- [16] RD48 collaboration, <http://rd48.web.cern.ch>, *ROSE/TN/2000-03*, *NIM A* **466** (2001) 308.
- [17] M. Huhtinen, Simulation of non-ionising energy loss and defect formation in silicon, *RD48 Technical Note 2001-02*, Cern(2001), submitted to NIM B.
- [18] *CERN/LHCC 98-6(1998)*, The CMS Collaboration, The Tracker Project Technical Design Report.
- [19] *CERN/LHCC 2000-16(2000)*, The CMS Collaboration, Addendum to the CMS Tracker TDR.
- [20] E. Focardi et al., The CMS silicon tracker, *NIM A* **453**(2000), 121.
- [21] *Pixel CMSIN1998/3*, R. Kaufmann and B. Henrich, Charge Drift in Silicon, 1998.
- [22] V. Eremin et al., Carrier drift mobility study in neutron irradiated high purity silicon, *NIM A* **362**(1995), 338–343.
- [23] T.J. Brodbeck et al., Carrier Mobilities in Irradiated Silicon,

*ROSE/TN/2000-09.*

- [24] C. Leroy et al., Charge transport in non-irradiated and irradiated silicon detectors, *NIM A*(1999), 90–102.
- [25] L.J. Beattie et al., The electric field in irradiated silicon detectors, *NIM A* 418(1998), 314–321.
- [26] G. Casse et al., Study of evolution of active volume in irradiated silicon detectors, *NIM A*(1999), 140–146.
- [27] D. Menichelli et al., Modelling of the observed double-junction effect, *NIM A* **426**(1999), 135–139.
- [28] RD39 Collaboration, *NIM A* **440** (2000) 5-16 and <http://rd39.web.cern.ch>, RD39 Status Report CERN/LHCC 2000-010, 06-Jan-2000.